

NJC

Accepted Manuscript



This is an *Accepted Manuscript*, which has been through the Royal Society of Chemistry peer review process and has been accepted for publication.

Accepted Manuscripts are published online shortly after acceptance, before technical editing, formatting and proof reading. Using this free service, authors can make their results available to the community, in citable form, before we publish the edited article. We will replace this *Accepted Manuscript* with the edited and formatted *Advance Article* as soon as it is available.

You can find more information about *Accepted Manuscripts* in the [Information for Authors](#).

Please note that technical editing may introduce minor changes to the text and/or graphics, which may alter content. The journal's standard [Terms & Conditions](#) and the [Ethical guidelines](#) still apply. In no event shall the Royal Society of Chemistry be held responsible for any errors or omissions in this *Accepted Manuscript* or any consequences arising from the use of any information it contains.

Cite this: DOI: 10.1039/c0xx00000x

www.rsc.org/xxxxxx

ARTICLE TYPE

Improved Catalytic Activity and Surface Electro-kinetics of Bimetallic Au-Ag Core-Shell Nanocomposites

Anila Monga and Bonamali Pal*

Received (in XXX, XXX) Xth XXXXXXXXX 20XX, Accepted Xth XXXXXXXXX 20XX

DOI: 10.1039/b000000x

This paper demonstrates the preparation of core-shell nanocomposites (NCs) of Au_{core}-Ag_{shell} (Au@Ag) and Ag_{core}-Au_{shell} (Ag@Au) for measuring their catalytic activity and electro-kinetic properties relative to their respective monometallic counterparts. A significant blue-shift (530 → 408 nm) and red-shift (420 → 550 nm) of the surface plasmon band for Au@Ag and Ag@Au NCs, respectively, was observed due to increased size of binary composites depending on the nature of core and shell material. The thickness of the deposited Ag shells varied from ~3-10 nm on Au core leading to the formation of Au@Ag NCs. On the other hand, the Ag core served as a sacrificial template, where Ag@Au NCs was converted to hollow Ag-Au alloy shells (~15 nm) because of the galvanic reaction between them due to the difference in their redox potential. Increased zeta potential of resulting Au@Ag (+57.8 mV) and hollow Ag-Au alloy shell (-20.13 mV) NCs in comparison to monometallic Au (-6.13 mV) and Ag nanospheres (-5.74 mV) was found due to surface passivation with aqueous AgNO₃ and AuCl₄⁻ solution, respectively. These bimetallic NCs exhibited ~2 times higher catalytic activity than the monometallic nanoparticles depending on shell thickness and the core of the respective metals for the nitrobenzene and 1,3-dinitrobenzene reduction.

Keywords: bimetallic NCs; Au@Ag core-shell morphology; hollow Ag-Au alloy; galvanic replacement; monometallic NPs

1. Introduction

The bimetallic nanocomposites (NCs) composed of two different metals are more significant than monometallic ones due to their improved electronic and optical properties, superior catalytic activity, high selectivity and stability emanating from bi-functional or synergistic effects.¹⁻⁴ The unique properties of bimetallic NCs over monometallic counterparts can be attributed to the reasons where⁵; (i) each metal element in bimetallic NCs promotes different elementary reaction steps leading to a bi-functional mechanism; (ii) the electronic or ligand effect^{6,7} where the addition of a second metal alters the electronic properties of the functioning sites of the first metal by electron transfer between the two different metals; (iii) an ensemble or geometric effect⁸ in which the coordination of atoms of a second metal to an atom of the first metal on the surface provides new geometries of active sites. In the past, much progress has been made for synthesis of NCs following a range of synthetic strategies, including co-reduction, galvanic replacement, thermal decomposition, seeded growth, photochemical, successive reduction, microwave, template, and electrochemical deposition methods.^{3,9-16} They can adopt either core-shell or alloy structures depending upon the synthetic approach employed.^{17,18} The core-shell NCs are attractive owing to the ability to increase the

functionality and stability of NPs by monitoring the nature of core and shell thickness. Moreover, the lattice mismatch between the core and shell material may induce the interfacial strain which has been shown to enhance catalytic rates in dual-metal systems. For example, Au/Pt core/shell exhibited enhanced electrocatalysis for oxygen reduction reaction.¹⁹ The Au/Pd core-shell heterostructures served as effective catalysts for catalyzing a Suzuki-coupling reaction.²⁰

Among bimetallic systems, the coinage metals (Au/Ag) nanostructures have been extensively explored due to their facile synthesis techniques, tunable surface plasmon (SP) band in the visible region, similar (FCC) crystal structure and lattice constants ($a = 0.479$ nm; Au and 0.486 nm; Ag) where Ag shells can be epitaxially formed in Au cores or vice-versa. Many NCs of Au-Ag, Au-Cu, Ag-Cu, Au-Pd, Cu-Au, and Cu-Pd, etc.^{13,14,21-26} of different morphology have been reported. Xia et al. recently synthesized Au@Ag core-shell nanocubes with controllable shell thicknesses.²⁷ The Au@Ag core-shell NCs of different shapes e.g., Octahedron, cube, decahedron, rod, wire, and icosahedrons using microwave-polyol method^{12,28,29} and core-shell (Au@Ag) and reverse core-shell (Ag@Au) NCs using β -CD were prepared by Pal et al.³⁰ By changing the nature of the core, shell-thicknesses and the core/shell ratio, the surface properties and catalytic activity of Au-Ag (core-shell) NCs can be manipulated

to be a consequence of different work functions of two metals. Since, the electronic distribution of both Au and Ag is different; the catalytic activity of shell atoms (Ag) can be electronically affected by the core atoms (Au) and vice-versa. Moreover, the coating of Au nanoparticles (NPs) core by Ag (shell) or reverse alters the nature of nanoparticle surface and hence its dispersion in liquid which governs the electro-kinetic properties i.e., Zeta-potential. Consequently, this work demonstrates the influence of core-shell Au@Ag and Ag@Au NCs on the optical properties, surface electro-kinetics and catalytic activity for model organic synthesis, as a function of their morphology, size distribution, the nature of the core and shell thickness relative to their monometallic counterparts.

2. Experimental

2.1. Materials

Chloroauric acid ($\text{HAuCl}_4 \cdot 3\text{H}_2\text{O}$), sodium borohydride (NaBH_4), ascorbic acid ($\text{C}_6\text{H}_8\text{O}_6$), sodium hydroxide (NaOH), polyvinylpyrrolidone (PVP), trisodium citrate ($\text{Na}_3\text{C}_6\text{H}_5\text{O}_7$), nitrobenzene ($\text{C}_6\text{H}_5\text{NO}_2$) and 1,3-dinitrobenzene ($\text{C}_6\text{H}_4\text{N}_2\text{O}_4$) were obtained from Loba Chemie, India. Silver nitrate (AgNO_3) was purchased from Fischer Scientific, India. All the chemicals were used as-received without any further purification. De-ionized water was obtained using an ultra-filtration system (Milli-Q, Millipore) with a measured conductivity above 35 mho cm^{-1} at 25°C .

2.2. Preparation of Au@Ag and Ag@Au NCs and their characterization techniques

The citrate-stabilized Au nanospheres (AuNS) and Ag nanospheres (AgNS) were prepared as reported³¹⁻³³ elsewhere. In brief, a solution of $\text{HAuCl}_4 \cdot 3\text{H}_2\text{O}$ or AgNO_3 ($70 \mu\text{l}$, 0.1 M) dissolved in water was injected into pre-heated aqueous solution of trisodium citrate (14 ml , 1.6 mM) at 100°C . After 20 min, the solution turned wine-red for Au and yellow for Ag, indicating the formation of corresponding metal NPs in the solution ($\text{pH} = 6.1$ to 6.2). The resulting washed citrate-capped AuNS (0.8 ml) solution was diluted with PVP (4 ml , $1 \text{ wt } \%$) into which different amount of AgNO_3 aqueous solution ($10\text{-}30 \mu\text{l}$, 0.01 M) was added. This was followed by adding ascorbic acid (0.1 ml , 0.1 M) and then NaOH (0.2 ml , 0.1 M) to initiate the deposition of Ag shell at alkaline pH ($\text{pH} = 10.0$ to 10.2) resulting in the formation of Au@Ag NCs.^{11,13} Similarly, the reverse core-shell NCs (Ag@Au) were synthesized by taking pre-synthesized citrate capped-Ag nanospheres (AgNS) as the core (demonstrated above). For each set of AgNS (0.8 ml) mixed with PVP (4 ml , $1 \text{ wt } \%$) and ascorbic acid (0.1 ml , 0.1 M), different amount of HAuCl_4^- aqueous solution ($10\text{-}30 \mu\text{l}$, 0.01 M) was added with simultaneous stirring resulting in the formation of Ag@Au NCs ($\text{pH} = 4.7\text{-}5.0$). The prepared bimetallic NCs were washed with distilled water by centrifugation (8000 RPM for 5 min) and dispersed in water. The core-shell NCs were characterized by UV-Vis absorption (Analytica Jena Specord 205) spectrophotometer, Transmission electron microscopy (TEM, Hitachi 7500, 2\AA , 120 KV), and Elemental detection spectroscopy (EDS). High-resolution TEM images and selected area electron diffraction (SAED) pattern were taken using FEI Technai F20 Transmission electron microscope. The

hydrodynamic size distribution of different NCs dispersed in water was determined by Brookhaven 90 plus Particle Size Analyzer at 25°C using Cumulant fitting, from which the effective diameter of particle is calculated. It contains a 15 mW solid state laser operating at 635 nm and an avalanche photodiode detector. The scattered light was detected at an angle of 90° . The zeta potential (ζ) was studied by taking 1.5 ml of NCs solution in a cuvette consisting of the palladium electrode mounted on a machined support using Brookhaven zeta plus at 25°C .

2.3. Catalytic activity

The comparative catalytic activity of bimetallic core-shell (Au@Ag and Ag@Au) NCs and their monometallic NPs were carried out by the reduction of nitrobenzene (NB) and 1,3-dinitrobenzene (DNB). In a typical reaction, $100 \mu\text{l}$ ice-cold NaBH_4 solution (0.01 M) was added to 5 ml Nitro-organic compounds (1 mM) and then, calculated amount of NCs was added. The reaction was monitored by measuring the absorption spectra at regular intervals of time (λ_{max} of NB $\sim 270 \text{ nm}$ and λ_{max} of DNB $\sim 240 \text{ nm}$). The products were further quantified by HPLC- Agilent 1120 compact LC equipped with a Qualisil BDS C-18 column ($250 \times 4.6 \text{ mm}$, $5 \mu\text{m}$) at $\lambda = 254 \text{ nm}$ with a flow rate of 1 ml/min and the eluent consisted of methanol 70: water 30 solutions. GC-MS analysis of reduction products was conducted with Bruker GC-45X with Scion MS system equipped with RTX-5 MS Sil column ($15 \text{ m} \times 0.25 \text{ mm} \times 0.25 \text{ mm}$).

3. Results and discussions

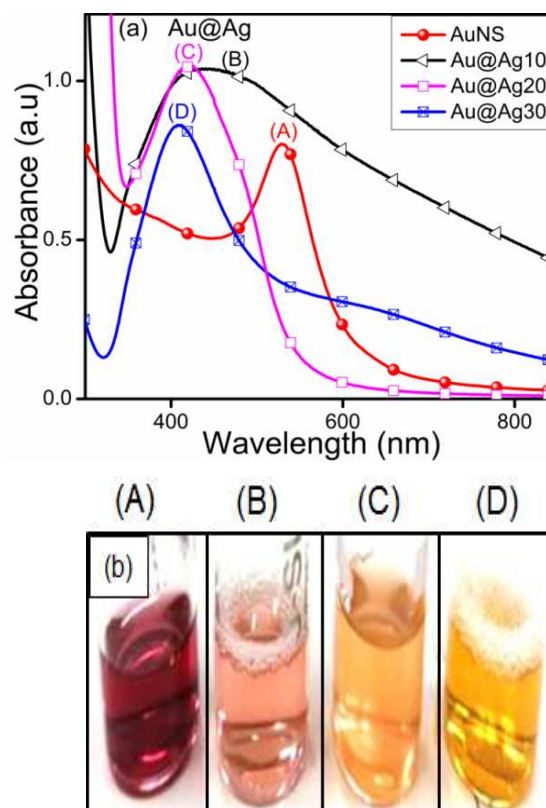


Fig 1. Effect of 0.01 M AgNO_3 ($10\text{-}30 \mu\text{l}$) deposition onto Au nanospheres for the observed (a) variation in the surface plasmon band of Au@Ag core-shell nanocomposites, and (b) their respective color changes.

The monometallic AuNS and AgNS were prepared by reducing Au and Ag ions with citrate, and then bimetallic core-shell Au@Ag and Ag@Au nanocomposites were obtained by deposition of varying amount Ag and Au ions over these as-prepared Au and Ag nanospheres, respectively. The resultant change in their surface structural morphology and various physicochemical properties including catalytic activity were comparatively investigated by different characterization techniques as below.

3.1. Optical properties

The characteristic surface plasmon (SP) band of AuNS (529 nm) blue-shifted to a broad peak at 447 nm and 419 nm of increased intensity upon addition of Ag^+ ions (10-20 μl , Figure 1a) accompanied by the color change from wine red to pink to orange as seen in Figure 1b. This indicated some morphological change in which AuNS were used as seeds for the controlled reduction of Ag^+ and thereby deposition of Ag-shell over the Au-core as observed from the absorbance measurements. With the progressive addition of Ag^+ ions (30 μl), a sharp absorption band corresponding to 408 nm having a yellow color appeared. At this point, the incident light could only penetrate Ag shell of a certain thickness and could not reach Au cores to excite its electron.²⁷ Therefore, it is presumed that AuNS are completely covered by Ag giving rise to $\text{Au}_{\text{core}}\text{-Ag}_{\text{shell}}$ (Au@Ag) NCs of different shell-thickness. These results are in good conformity with the reported blue shifting of the SP band for AuNS from 520 nm to 438 nm and 402 nm with increasing Ag-shell thickness.³⁰

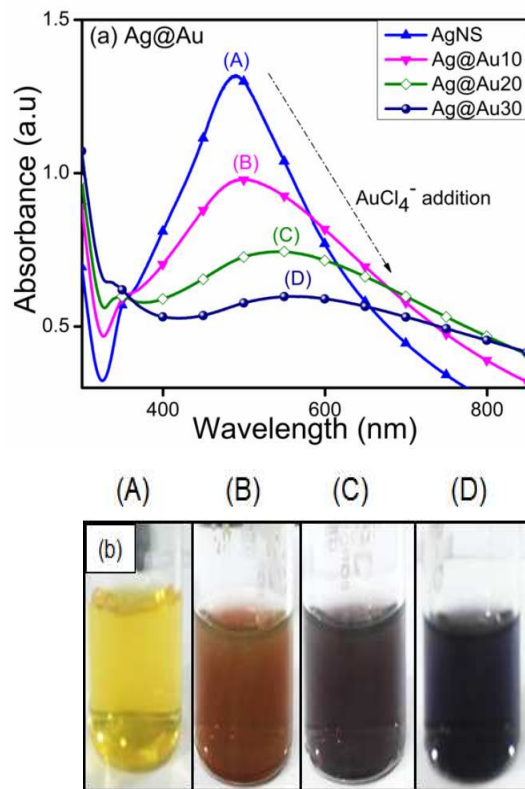
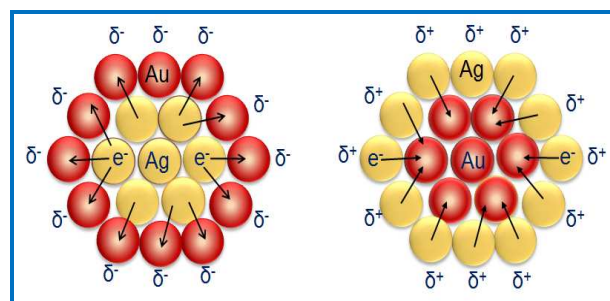


Fig 2. Effect of 0.01 $\text{MHAuCl}_4 \cdot 3\text{H}_2\text{O}$ (10-30 μl) deposition onto Ag nanospheres for the observed (a) variation in the surface plasmon band of Ag@Au core-shell nanocomposites, and (b) their respective color changes.

In contrast to AuNS, the SP band of AgNS (414 nm) decreased gradually and became broader with a peak position shifting to longer wavelengths, 490 nm to 508 nm and 550 nm through the increasing addition of HAuCl_4^- ions aqueous solution (Figure 2a). This observation is consistent with the report where the formation of hollow Ag-Au NCs takes place via replacement of Ag by Au.³⁴ Due to the progressive galvanic replacement reaction, Au is deposited on NPs surface and the cavity size in hollow particles increases with reaction resulting in a red-shift³⁵ in the SP band of hollow Ag-Au NCs. This morphological transformation was further evidenced by the color change from yellow to light orange to purple and blue as shown in Figure 2b. The above experiment was repeated with AuNS and AgNS of different sizes as observed from their SP band in *Figure S1* in electronic supplementary information (*ESI*) and almost similar results were obtained. In *ESI-Figure S1a*, the SP band of AuNS (518 nm) blue-shifted to a broad peak at 460 nm, whereas AgNS (414 nm) red-shifted to a broadened peak at 606 nm after treatment with Ag^+ and HAuCl_4^- (20 μl , 0.01 M), respectively. The absorbance peak of AuNS (528 nm) and AgNS (400 nm) became sharp at 420 nm and 558 nm after coating with higher amount Ag^+ and HAuCl_4^- (30 μl , 0.01 M), respectively, as shown in *ESI-Figure S1b*.

3.2. Electro-kinetic parameters

When NPs are dispersed in an aqueous solution, there is adsorption or surface ionization of cations or anions, which results in the formation of electrical double layer leading to the development of new surface charge measured by Zeta potential (ζ). Here, the measured zeta potential of unwashed citrate-capped AuNS (-22.5 mV) and AgNS (-28.79 mV) was found to be negatively charged probably due to the presence of surface adsorbed and free citrate ions in their aqueous suspension. However, after washing with de-ionized water, the zeta potential of bare AuNS (-6.13 mV) and AgNS (-5.74 mV) was notably reduced (Figure 3).³⁶ The citrate capped-AuNS and AgNS are probably stabilized through steric repulsions as reported³⁷⁻⁴⁰ due to the presence of coordinated/adsorbed citrates along with dangling citrate species which are not in direct contact with the metal surface of Au or Ag NPs. As a result, intermolecular interactions take place between the adsorbed citrate and dangling citrate anion by COOH hydrogen bonds and hence forms citrate multilayer on the NPs surface. This provides steric repulsion between citrate layers present on the adjacent NPs, and help in NPs dispersion stability in solution.



Scheme 1. Schematic illustration of electron charge transfer.

The zeta potential for bimetallic Au@Ag and Ag@Au NCs was measured in their aqueous medium having core: shell atomic ratio = 1:0.2, 1:0.5, and 1:0.7 as calculated in *ESI-Table S2 and S3*. The Ag⁺ deposition on the AuNS surface led to the positive (+30.3 mV) surface charge indicating the bare AuNS are chemically modified through the absorbed charged Ag-shell as shown in Figure 3a. Further, it was observed that the zeta potential became more positive (+40.7 mV to +57.8 mV), probably due to the increasing Ag-shell thickness with gradual addition of Ag⁺. In case of AgNS, the surface charge became more negative³⁶ (-13.35 mV to -20.13 mV) after progressive addition of HAuCl₄ as shown in Figure 3b. This charge alteration might be due to the electron charge donation from Ag with low ionization potential (7.58 eV) to Au with high ionization potential (9.22 eV)⁴¹⁻⁴³ as depicted in Scheme 1. This results in accumulation of positive charge on Ag-shell and negative charge on Au-shell in case of Au@Ag and Ag@Au NCs, respectively, as evidenced by the above results in agreement with the previous report.⁴³

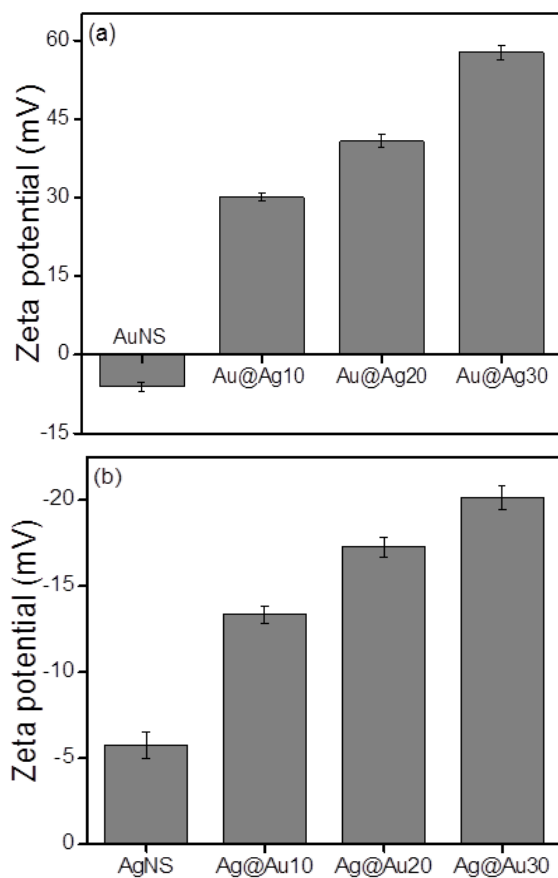


Fig 3. Electro-kinetic parameters of (a) Au nanospheres, and (b) Ag nanospheres after deposition of 0.01 M AgNO₃ and 0.01 M HAuCl₄·3H₂O (10-30 μl), respectively.

3.3. Particle size distribution

The coating or deposition of second metal (shell) on core NPs may lead to the change in the particle size of bare NPs. Here, the Au-core of particular size (25 nm) was used for the deposition of an Ag layer of varying thickness as a function of concentration of

Ag⁺ ions. The Ag⁺ ions are first adsorbed on the surface of AuNS which then undergoes reduction in the presence of a weak reducing agent, ascorbic acid, so that the reduction takes place on the surface of existing metallic surfaces. Subsequently, the resultant NCs may lead to the increment of size compared to bare NPs (Scheme 2) due to the growing thickness of Ag-shell irrespective of the Au-core size which can be evidenced by the DLS particle size distribution.⁴⁴ It revealed that the average hydrodynamic diameter of AuNS (25 nm) upon addition of Ag⁺ exhibited an increase in particle diameter (31 nm) signifying the successful coating of Ag layer on AuNS as shown in Figure 4a. Further, the successive addition of Ag⁺ into AuNS, resulted in a progressive increase in particle diameter (41 nm to 62 nm) indicating the Ag-shell growth of higher thickness depending upon its added concentration. Similarly, Figure 4b shows that the average hydrodynamic diameter of AgNS (21 nm) subsequently, upon addition of different amount of HAuCl₄ lead to the gradual increase in particle diameter (33 nm to 58 nm). The AgNS act as a sacrificial template for the growth of Au layer and resulted in the formation of hollow Ag-Au alloy of increased cavity size due to the galvanic displacement reaction as depicted in Scheme 2. The observed hydrodynamic diameter is found to be greater than the TEM size due to the presence of the hydration layer while estimating the size by DLS. The DLS autocorrelation functions and its corresponding fit are demonstrated in supporting information (*ESI-S4-S6*).

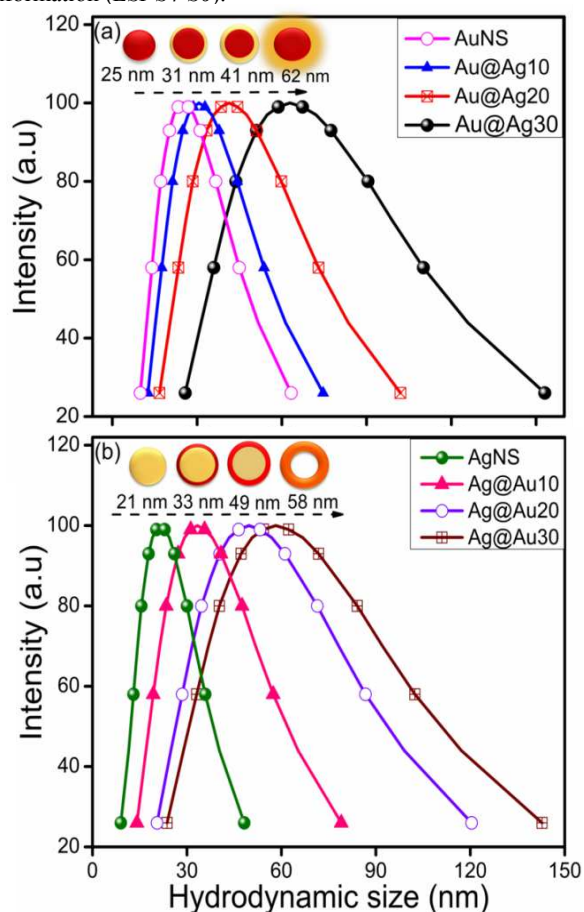
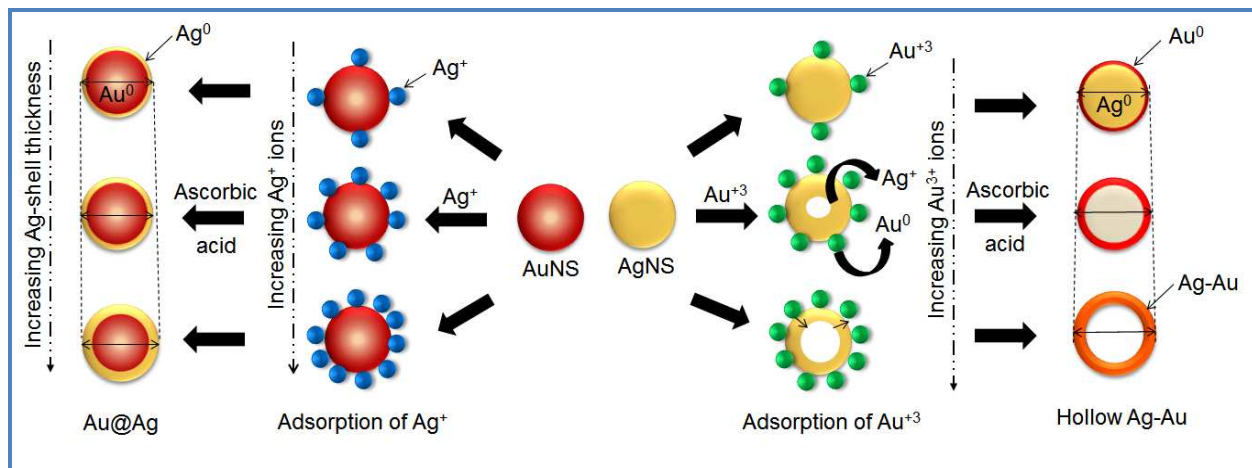


Fig 4. DLS particle size distribution after deposition of 10-30 μl (0.01 M) (a) AgNO₃ over Au nanospheres, and (b) HAuCl₄·3H₂O over Ag nanospheres.



Scheme 2. Schematic representation of the formation of Au-Ag bimetallic nanostructures.

3.4. Morphological studies

TEM analysis revealed that the bare AuNS of diameter = 10-16 nm (Figure 5a) served as seeds for Ag growth on its surface. The gradual addition of Ag^+ on pre-synthesized AuNS led to a coating of an Ag layer of thickness ~ 3 -4 nm as shown in Figure 5b,c. This is in good agreement with the structural configuration of core-shell, i.e., Au@Ag NCs where the dark core is attributed to Au and light shell corresponds to Ag. The Ag shell was observed to become thicker (~ 8 -10 nm), diffused and non-uniform with the addition of higher amount of Ag^+ ions giving rise to irregular shape (diameter ~ 20 nm) as seen in Figure 5d. These observations are in accordance with the reports where Ag coating becomes anisotropic with increasing thickness of Ag shell and the shape of Au nanorods approached being a non-regular.^{14,45} Elemental analysis further confirmed that both Au and Ag are present in Au@Ag NCs as shown in EDS spectra, *ESI-Figure S7a*. The HRTEM image of the as-prepared Au@Ag NCs of size ~ 14 -19 nm with a thickness of Ag shell ~ 2 -3 nm is shown in Figure 6a,b.

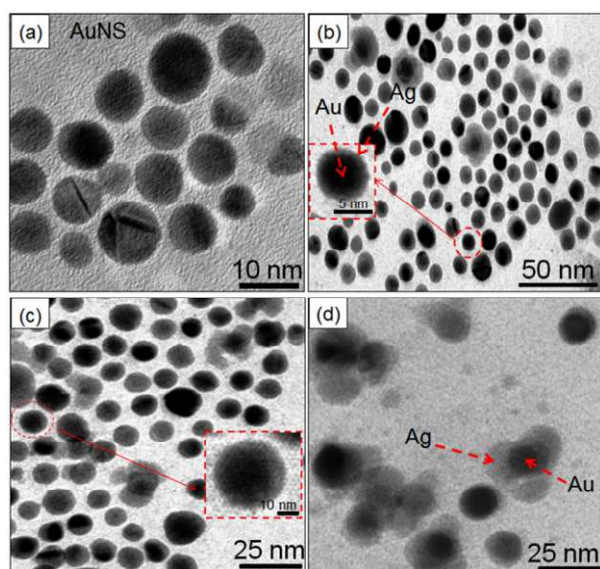


Fig 5. TEM images of (a) Au nanospheres, and (b-d) Au@Ag core-shell nanocomposites of varying Ag-shell thickness (ca. ~ 3 -10 nm).

The measured fringes spacing are 2.3 Å and 1.4 Å, which corresponded well with the (111) plane of the FCC Au (2.355 Å, Figure 6c) and (110) plane of Ag (1.44 Å, JCPDS card no. 04-07484, inset of Figure 6c), respectively. Similarly, another HRTEM and the SAED pattern (*ESI-Figure S8*) of the Au@Ag NCs confirmed the planes (110) of Ag and (111) of Au NPs. These results indicated the presence of both Au and Ag supporting the formation of Au core with Ag shell as suggested by the previous report.⁴⁶

On the other hand, the different morphology of AgNS was observed via the galvanic displacement reaction between AgNS and HAuCl_4^- as seen in Figure 7. The bare AgNS (diameter = 10-11 nm, Figure 7a) was uniformly coated with an Au-layer (thickness = ~ 2.9 nm) upon treatment with lower amount (10 μl)

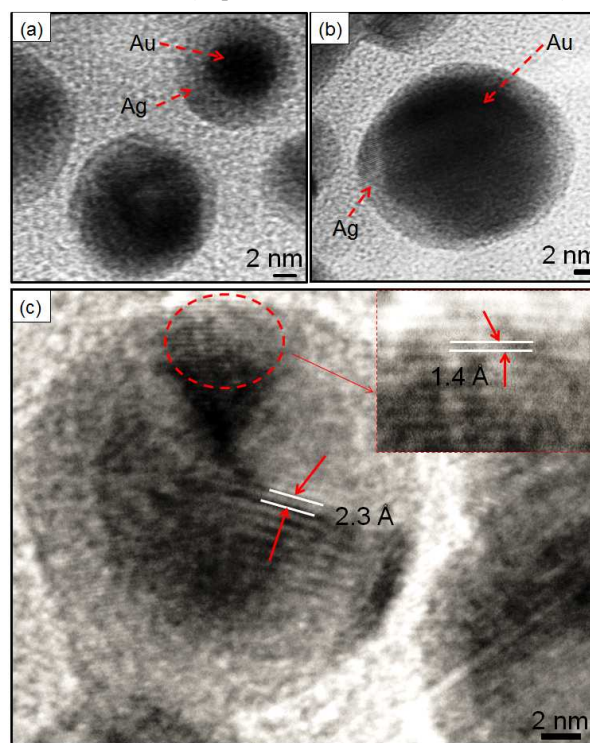


Fig 6. HRTEM image of Au@Ag core-shell nanocomposites.

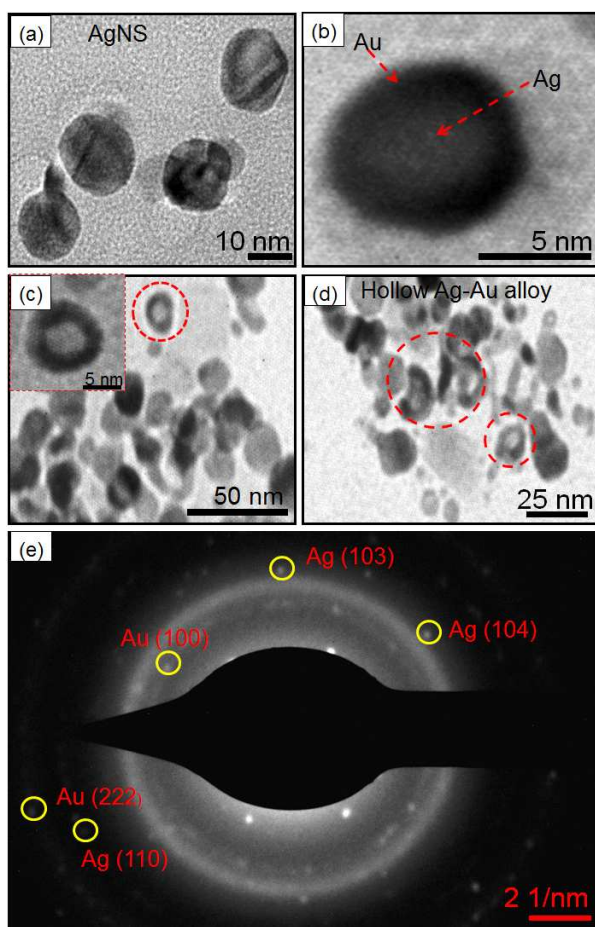


Fig 7. TEM images of (a) Ag nanospheres, (b-d) Ag@Au core-shell nanocomposites obtained by deposition of 10-30 μl of $\text{HAuCl}_4 \cdot 3\text{H}_2\text{O}$ (0.01 M), and (e) SAED pattern obtained from image-(c).

of HAuCl_4^- as noted in Figure 7b. With increasing Au content, the Ag particles are oxidized into Ag^+ ions due to the higher reduction potential of Au^{+3}/Au (0.99 V) than Ag^+/Ag (0.80 V). As a result, the growth of Au layer on the surface of Ag template takes place leading to the formation of Ag-Au alloys (Figure 7c) of diameter ~ 10 -12 nm. The difference in the rates of diffusion of Ag atoms outward and that of AuCl_4^- ions inward started the formation of hollow spaces (~ 5 nm) to produce Ag-Au alloy nanorings (diameter = 13-15 nm, Figure 7d) with increased cavity size as reported by many groups^{10,35,47} in which different shapes (cubes, spheres, wires, etc.) of Ag-Au bimetallic NCs are prepared. The resulting hollow NCs were observed to compose of both metals as evidenced by the presence of Ag and Au in EDS analysis (*ESI-Figure S7b*). Further, the SAED pattern supported the existence of the planes (111) of Au and (110) of Ag particles as depicted in Figure 7e.⁴⁸

3.5. Catalytic activity

The absorption spectra for the reduction of NB (270 nm) to aniline (AN) by NaBH_4 exhibited insignificant changes in the absence of AuNS up to 120 min as shown in *ESI-Figure S9a*. However, with the addition of AuNS (size = 10-16 nm), the reaction rate was accelerated and the absorption band intensity corresponding to NB at 270 nm was gradually reduced with the

simultaneous evolution of new absorption band at 234 nm, characteristic of the AN formation (Figure 8a). The time course studies (Figure 8b) displayed that the Au@Ag and hollow Ag-Au alloy NCs exhibited higher yield of AN i.e., 50% and 72%, respectively, within 15-30 min as compared to bare AuNS (42%) and AgNS (20%) within 40-50 min. The superior catalytic activity of bimetallic NCs can be explained due to the modification of the electronic structures^{2,49,50} in two metals which results in broader d-band shifted towards the Fermi-level due to the charge rearrangement. This is in agreement with the report⁵¹ where the polyelectrolyte multilayer supported Au@Ag ($k=0.18 \text{ min}^{-1}$) NCs showed higher catalytic activity for the reduction of *p*-nitrophenol to *p*-aminophenol by NaBH_4 than the corresponding monometallic AuNS ($k=0.019 \text{ min}^{-1}$) and AgNS ($k=0.069 \text{ min}^{-1}$) due to synergistic effect. Bimetallic synergistic effect exhibits a dramatic improvement in catalytic activity and selectivity in contrast to monometallic counterparts.^{3,45} The introduction of second metal (shell) over the surface of another metal NP core leads to the structural change and formation of boundaries two metal atoms. Consequently, electronic charge transfer occurs between two metals leading to a change in the

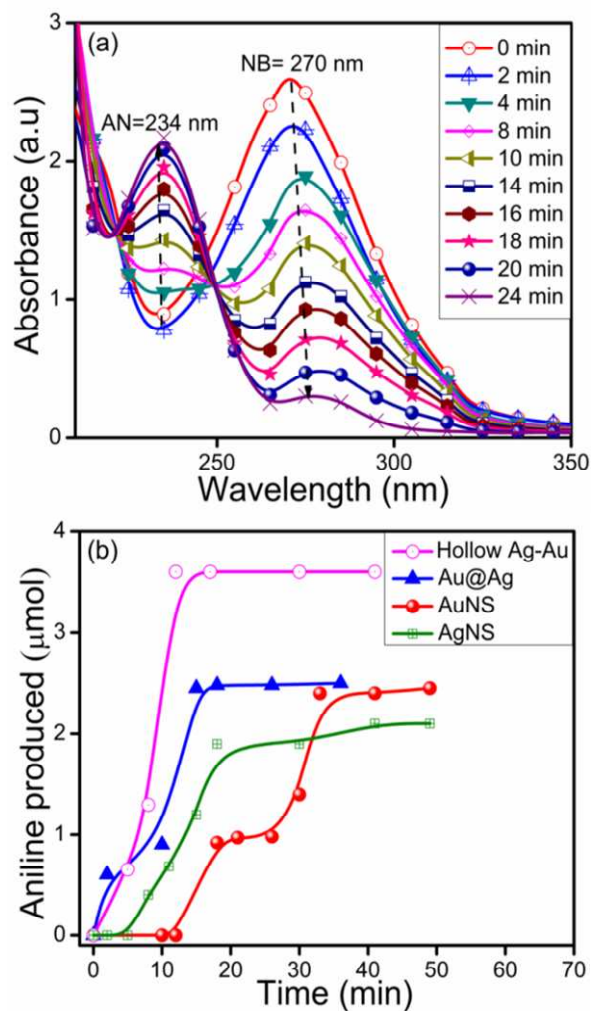


Fig 8. Changes in absorption spectra during nitrobenzene reduction by (a) Au nanospheres (size ~ 10 -16 nm), and (b) time course graph of aniline formation by various mono/bimetallic nanostructures.

electron density on the resultant bimetallic NP which may promote the reduction process more efficiently.^{41,42}

The effect of electron withdrawing group on rate of reduction was studied by carrying out the reduction of 1,3-DNB to 3-nitroaniline (NA) and phenylenediamine (PDA) by core-shell NCs of varying shell-thickness. The reduction process led to the decrease in absorption spectra of DNB (240 nm) with the progressive rise of peak at 285 nm corresponding to a PDA (*ESI-Figure S9b*). But the quantitative analysis (HPLC, *ESI-Figures S10 and S11*) revealed the formation of another product also i.e., NA along with PDA. Figure 9a shows that the yield of PDA was increased to 70% with addition of Ag⁺ (10 μ l) to AuNS (Au@Ag10) in contrast to monometallic AuNS (45%). However, the further increase in the Ag amount (20 and 30 μ l) on Au-core i.e., Au@Ag20 (PDA = 52%) and Au@Ag30 NCs (PDA = 48%), respectively, dramatically decreased the catalytic activity. This can be ascribed to the weaker electronic effect between distant Au-core and Ag-shell, resulting from growing Ag-shell thickness. Atee-Esfahani et al.⁵² even reported that the Pt surface cannot

work well as an electro-active surface for methanol oxidation with higher Pt/Au molar ratio or without an Au core. On the other hand, the catalytic reduction by AgNS to the growing amount of HAuCl₄⁻ (10-30 μ l) showed progressive increase in PDA yield as seen in Figure 9b. The hollow Ag-Au alloy (PDA = 82%) exhibited highest catalytic activity among the various Ag@Au core-shell NCs (PDA = 61-64%) and bare AgNS (PDA = 36%) due to their increased surface areas and reduced densities. In this, the inner surface of the hollow shell may provide more bonding sites for the chemical reaction.⁵³⁻⁵⁶ In addition, the different arrangement of Ag and Au in the catalysts (either as core or shell) also played a role in affecting the catalytic efficiency due to which Ag@Au NCs exhibited better catalytic activity than Au@Ag NCs.³⁸ This is because the electronic charge could transfer from Ag-core to Au-shell in view of their ionization potential, leading to an increase in electron density on directly exposed Au NPs surface to the solution promoting the reduction more efficient as reported earlier.^{42,50} Further, GC-MS analysis of reaction product obtained after reduction of DNB with NCs, qualitatively evidences the formation of PDA, R_t = 11.4 and 12.1 min (1 and 2) and NA, R_t = 14.6 and 15.3 min (4 and 6) from DNB, R_t = 14.0 and 14.7 min (3 and 5) as noted in Figures 10a-b and *ESI-Figure S12*. The mass spectrum (Figure 10c-h) showed the peak at m = 108 for 1 and 2 and m = 138 for 4 and 6 compounds confirming the PDA and NA formation. The other peak at m = 168 for 3 and 5 compounds corresponding to DNB was also observed due to its incomplete conversion. Among DNB and NB, the higher reduction rate was found in DNB probably due to the reason that the insertion of second -NO₂ group (e⁻ withdrawing group) into nitrobenzene might lower the electron density on other -NO₂ group favoring rapid conversion of -NO₂ into -NH₂ group. Hence, the conversion of nitro-aromatic compounds to their respective products enhanced by ~2 times using bimetallic NCs in contrast to their monometallic counterparts. Therefore, through the optimization of shell-thickness and nature of the core, the catalytic efficiency can be enhanced for the other reduction processes.

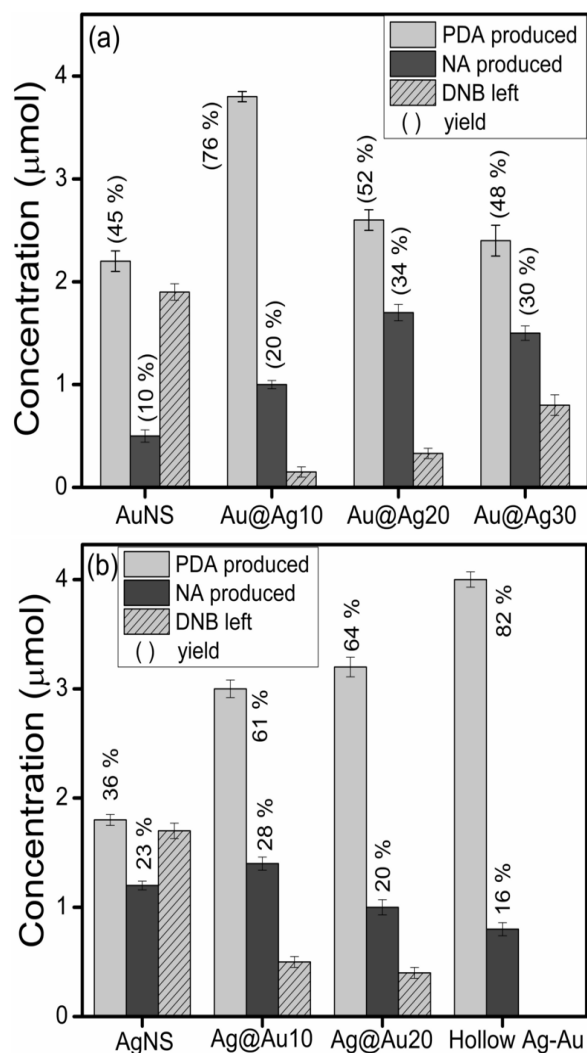


Fig 9. Amount of 3-nitroaniline (NA) and 1,3-phenylenediamine (PDA) produced from 1,3-dinitrobenzene (DNB) reduction by different mono and bimetallic (a) Au@Ag, and (b) Ag@Au core-shell nanocomposites.

4. Conclusions

In summary, the effects of the nature of coinage metal core as well as shell-thickness have been studied on the variation of surface electro-kinetic and catalytic properties as compared to their monometallic counterparts. The Ag shell (or Au) thicknesses on Au (or Ag) cores can be easily tuned by controlling the concentration of starting precursor solutions. As a result, the synergistic effect of mixed band energy of two different coinage metals, active catalytic active sites and preferred surface orientation for adsorption of reacting substrates may alter catalytic efficiency. These bimetallic nanocolloids of coinage metals are used for improving the catalytic activity for Nitro-organics reduction reaction where the selectivity and yield of the products can be tuned depending on their composition and surface morphology.

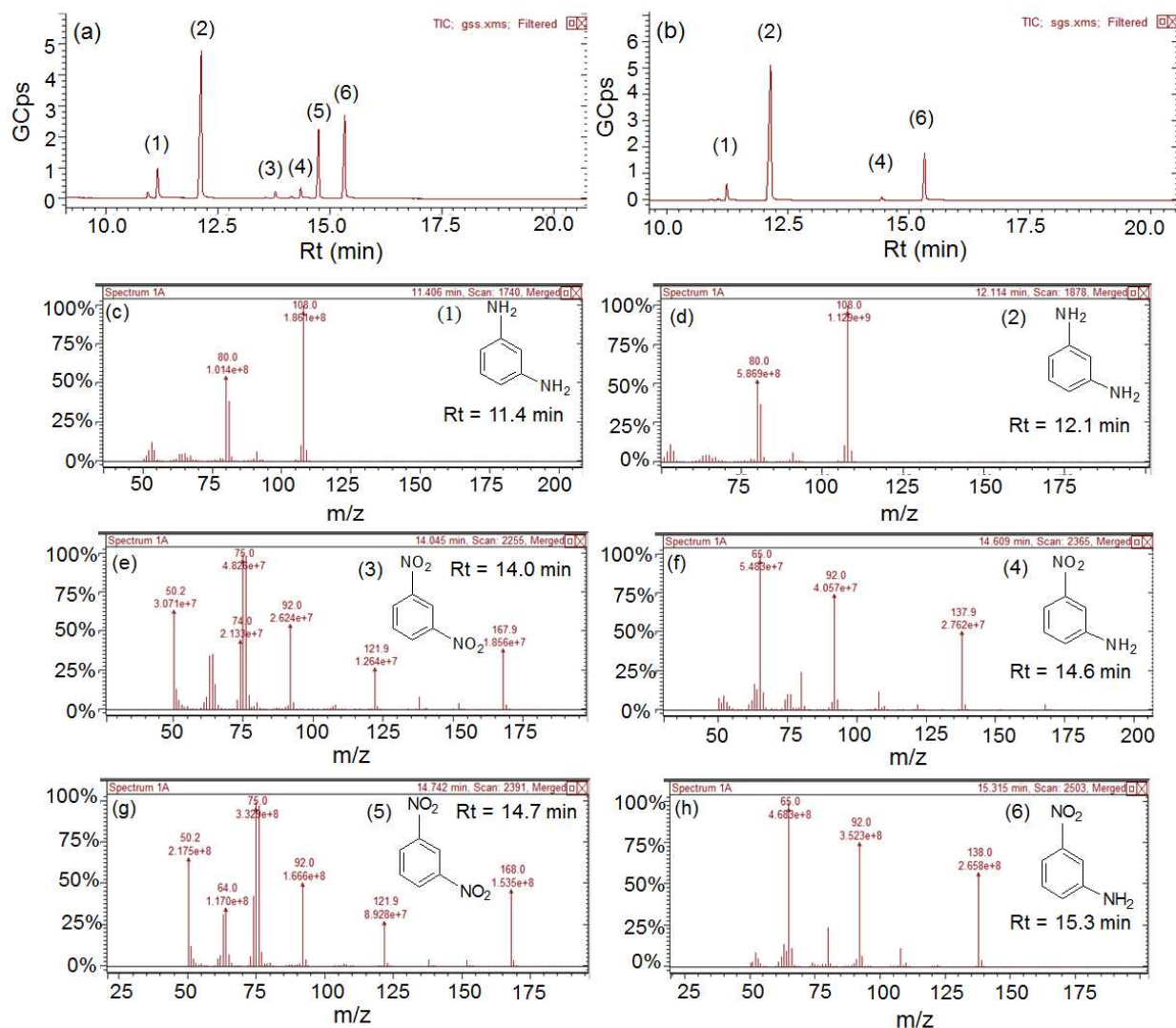


Fig 10. Gas chromatograph of reaction product after reduction of 1,3-dinitrobenzene by (a) Au@Ag core-shell nanocomposites, (b) hollow Au-Ag alloy, and (c-h) their corresponding mass spectra.

Acknowledgements

We acknowledge Dr. B. N. Chudasama (School of Physics and Material Science, Thapar University) for Zeta potential and DLS measurement. We would also like to thank to Sophisticated Analytical Instrumentation Facility (IIT Bombay) for TEM analysis and NIPER, Mohali (India) for HRTEM analysis. We acknowledge CSIR for the financial support.

Notes and references

School of Chemistry and Biochemistry, Thapar University, Patiala-147004, Punjab, India

Fax: +91-175-236-4498; Tel: +91-175-239-3128

Email: bpal@thapar.edu

Electronic Supplementary Information (ESI) available: [UV-Vis absorption spectra, EDS spectra, HRTEM and SAED pattern of Au@Ag and Ag@Au NCs, Calculation of atomic ratio of Au/Ag, Autocorrelation spectra for DLS particle size distribution, UV-Vis absorption spectra,

HPLC and GC analysis for the reduction of NB and 1,3-DNB]. See DOI: 10.1039/b000000x/

- 20 (1) N. Toshima and T. Yonezawa, *New J. Chem.*, 1998, **22**, 1179–1201.
- (2) D. S. Wang and Y. D. Li, *Adv. Mater.*, 2011, **23**, 1044–1060.
- (3) H. L. Jiang and Q. Xu, *J. Mater. Chem.*, 2011, **21**, 13705–13725.
- (4) R. Ferrando, J. Jellinek and R. L. Johnston, *Chem. Rev.*, 2008, **108**, 845–910.
- 25 (5) F. Tao, *Chem. Soc. Rev.*, 2012, **41**, 7977–7979.
- (6) C. C. Tyson, A. Bzowski, P. Kristof, M. Kuhn, R. Sammynaiken and T. K. Sham, *Phys. Rev. B*, 1992, **45**, 8924–8928.
- (7) S. Nishimura, A. T. N. Dao, D. Mott, K. Ebitani and S. Maenosono, *J. Phys. Chem. C*, 2012, **116**, 4511–4516.
- 30 (8) S. Sakong, C. Mosch and A. Gross, *Phys. Chem. Chem. Phys.*, 2007, **9**, 2216–2225.
- (9) M. Kaushik, M. Mandal, N. Pradhan and T. Pal, *Nano Lett.*, 2001, **1**, 319–322.
- (10) Y. Sun and Y. Xia, *J. Am. Chem. Soc.*, 2004, **126**, 3892–3901
- 35 (11) B. Rodriguez-Gonzalez, A. Burrows, M. Watanabe, C. J. Kiely and L. M. L. Marzan, *J. Mater. Chem.*, 2005, **15**, 1755–1759.
- (12) M. Tsuji, N. Miyamae, S. Lim, K. Kimura, X. Zhang, S. Hikino and M. Nishio, *Cryst. Growth Des.*, 2006, **6**, 1801–1807.

- (13) M. Liu and P. Guyot-Sionnest, *J. Phys. Chem. B*, 2004, **108**, 5882–5888.
- (14) Y. Xiang, X. Wu, D. Liu, Z. Li, W. Chu, L. Feng, K. Zhang, W. Zhou and S. Xie, *Langmuir*, 2008, **24**, 3465–3470.
- (15) M. J. Alam and M. Tsuji, *Cryst. Eng. Comm.*, 2011, **13**, 6499–6506.
- (16) M. Tsuji, N. Nakamura, M. Ogino, K. Ikeda and M. Matsunaga, *Cryst. Eng. Comm.*, 2012, **14**, 7639–7647.
- (17) M. P. Mallin and C. J. Murphy, *Nano Lett.*, 2002, **2**, 1235–1237.
- (18) L. Rivas, S. Sanchez-Cortes, J. V. Garcia-Ramos and G. Morcillo, *Langmuir*, 2000, **16**, 9722–9728.
- (19) L. Chen, L. Kuai and B. Geng, *Cryst. Eng. Comm.*, 2013, **15**, 2133–2136.
- (20) C. W. Yang, K. Chanda, P. H. Lin, Y. N. Wang, C. W. Liao, and M. H. Huang *J. Am. Chem. Soc.* 2011, **133**, 19993–20000.
- (21) M. Sakamoto, T. Tachikawa, M. Fujitsuka and T. Majima, *Adv. Funct. Mater.*, 2007, **17**, 857–862.
- (22) T. Nakamura, Y. Tsukahara, T. Yamauchi, T. Sakata, H. Mori and Y. Wada, *Chem. Lett.*, 2007, **36**, 154–155.
- (23) M. Tsuji, S. Hikino, R. Tanabe, M. Matsunaga and Y. Sano, *Cryst. Eng. Comm.*, 2010, **12**, 3900–3908.
- (24) Y. Ding, F. Fan, Z. Tian and Z. L. Wang, *J. Am. Chem. Soc.*, 2010, **132**, 12480–12486.
- (25) J. Xu, A. R. Wilson, A. R. Rathmell, J. Howe, M. Chi and B. J. Wiley, *ACS Nano*, 2011, **5**, 6119–6127.
- (26) S. Chen, S. V. Jenkins, J. Tao, Y. Zhu and J. Chen, *J. Phys. Chem. C*, 2013, **117**, 8924–8932.
- (27) Y. Ma, W. Li, E. C. Cho, Z. Li, T. Yu, J. Zeng, Z. Xie and Y. Xia, *ACS Nano*, 2010, **4**, 6725–6734.
- (28) M. Tsuji, R. Matsuo, P. Jiang, N. Miyamae, D. Ueyama, M. Nishio, S. Hikino, H. Kumagae, K. S. N. Kamarudin and X. L. Tang, *Cryst. Growth Des.*, 2008, **8**, 2528–2536.
- (29) M. Tsuji, M. Ogino, M. Matsunaga, N. Miyamae, R. Matsuo, M. Nishio and M. J. Alam, *Cryst. Growth Des.*, 2010, **10**, 4085–4090.
- (30) S. Pande, S. K. Ghosh, S. Praharaj, S. Panigrahi, S. Basu, S. Jana, A. Pal, T. Tsukuda and T. Pal, *J. Phys. Chem. C*, 2007, **111**, 10806–10813.
- (31) N. G. Bastus, J. Comenge and V. Puentes, *Langmuir*, 2011, **27**, 11098–11105.
- (32) G. Kawamura, Y. Yang and M. Nogami, *J. Phys. Chem. C*, 2008, **112**, 10632–10636.
- (33) I. Ojea-Jimenez and V. Puentes, *J. Am. Chem. Soc.*, 2009, **131**, 13320–13327.
- (34) X. Zhang, G. Zhang, B. Zhang and Z. Su, *Langmuir*, 2013, **29**, 6722–6727.
- (35) C. Shankar, A. T. N. Dao, P. Singh, K. Higashimine, D. M. Mott and S. Maenosono, *Nanotechnology*, 2012, **23**, 245704.
- (36) S. H. Wang, C. W. Lee, A. Chiou and P. K. Wei, *J. Nanobiotechnology*, 2010, **8**, 33–45.
- (37) J. W. Park and J. S. S. Parry, *J. Am. Chem. Soc.*, 2014, **136**, 1907–1921.
- (38) S. Biggs, P. Mulvaney, C. F. Zukoski and F. Grieser, *J. Am. Chem. Soc.*, 1994, **116**, 9150–9157.
- (39) P. Wagener, A. Schwenke and S. Barcikowski, *Langmuir*, 2012, **28**, 6132–6140.
- (40) C. H. Munro, W. E. Smith, M. Garner, J. Clarkson and P. C. White, *Langmuir*, 1995, **11**, 3712–3720.
- (41) H. Zhanga and N. Toshima, *Catal. Sci. Technol.*, 2013, **3**, 268–278.
- (42) S. Tokonami, N. Morita, K. Takasaki and N. Toshima, *J. Phys. Chem. C*, 2010, **114**, 10336–10341.
- (43) S. Nishimura, A. T. N. Dao, D. Mott, K. Ebitani and S. Maenosono, *J. Phys. Chem. C*, 2012, **116**, 4511–4516.
- (44) M. Kahraman, O. Aydin and M. Culha, *Plasmonics*, 2009, **4**, 293–301.
- (45) Q. Fu, D. G. Zhang, M. F. Yi, X. X. Wang, Y. K. Chen, P. Wang and H. Ming, *J. Opt.*, 2012, **14**, 085001.
- (46) H. F. Zarick, W. R. Erwin, J. Aufrecht, A. Coppola, B. R. Rogers, C. L. Pint and R. Bardhan, *J. Mater. Chem. A*, 2014, **2**, 7088–7098.
- (47) S. W. Hsu, K. On, B. Gao and A. R. Tao, *Langmuir*, 2011, **27**, 8494–8499.
- (48) T. Ghosh, B. Satpati and D. Senapati, *J. Mater. Chem. C*, 2014, **2**, 2439–2447.
- (49) P. Venkatesan and J. Santhanalakshmi, *Langmuir*, 2010, **26**, 12225–12229.
- (50) X. Guo, Q. Zhang, Y. Sun, Q. Zhao and J. Yang, *ACS Nano*, 2012, **6**, 1165–1175.
- (51) X. Zhang and Z. Su, *Adv. Mater.*, 2012, **24**, 4574–4577.
- (52) H. Atae-Esfahani, L. Wang, Y. Nemoto and Y. Yamauchi, *Chem. Mater.*, 2010, **22**, 6310–6318.
- (53) H. Wu, P. Wang, H. He and Y. Jin, *Nano Res.*, 2012, **5**, 135–144.
- (54) M. R. Kim, D. K. Lee and D. J. Jang, *Appl. Catal. B: Environ.*, 2011, **103**, 253–260.
- (55) H. M. Chen, R. S. Liu, M. Y. Lo, S. C. Chang, L. D. Tsai, Y. M. Peng and J. F. Lee, *J. Phys. Chem. C*, 2008, **112**, 7522–7526.
- (56) J. Zeng, Q. Zhang, J. Chen and Y. Xia, *Nano Lett.*, 2010, **10**, 30–35.